Supplementary information for Improving Reanalysis Hub-Height Wind Speeds and Wind Shear Across Large Spatial Domains Using Near-Surface Observational Networks

Freddy Houndekindo[1*], Taha B.M.J. Ouarda[1]

[1]Canada Research Chair in Statistical Hydro-Climatology, Institut national de la recherche scientifique, Centre Eau Terre Environnement, 490 de la Couronne, Québec, QC, G1K 9A9, Canada

*Corresponding author: Freddy Houndekindo

490, Couronne street, Québec, QC, G1K 9A9, Canada

Tel : +1 418-654-3842

E-mail : freddy.houndekindo@inrs.ca

Table S1. Information of the Tall Tower Dataset stations used in the study as reference for validation.

Station name	Longitude (° West)	Latitude (° North)	height above sea level (m)	Standard deviation of orography height
BROOKHAVEN	-84.337	33.865	308.052	14.759
BUTLER GRADE	-118.683	45.95	543.625	95.134
CHINOOK	-119.534	45.833	156.044	62.942
KENNEWICK	-119.117	46.1	595.388	105.895
MEGLER	-123.877	46.266	338.901	22.062
NWTC M2	-105.235	39.911	1857.351	190.058
NWTC M4	-105.225	39.906	1847.286	190.058
NWTC M5	-105.225	39.206	2338.231	223.05
OAK RIDGE	-84.324	35.926	262.289	81.149
OSU	-84.714	45.56	248.565	30.83
PARK FALLS	-90.273	45.945	471.03	10.14
SEVEN MILE	-121.267	45.634	289.723	186.304
TROUTDALE	-122.402	45.558	6.477	92.689
WASCO	-120.767	45.5	630.692	110.676

Notes: The height above sea level was estimated from a digital elevation model (DEM). The Standard deviation of orography height is a parameter that characterizes terrain variability unresolved by the ERA5 model grid.

Table S2. Assigned aerodynamic surface roughness length (z_0) to land cover classes. The table presents the land cover classes and pixel ID derived from The North American land cover map, along with the assigned z_0.

Land cover class	**Pixel ID**	**z_0 (in meter)**
Temperate or sub-polar needleleaf forest	1	2.0
Sub-polar taiga needleleaf forest	2	2.0
Tropical or sub-tropical broadleaf evergreen forest	3	2.0
Temperate or sub-polar broadleaf deciduous forest	5	2.0
Tropical or sub-tropical shrubland (perennial plants)	7	0.5
Temperate or sub-polar Shrubland	8	0.5
Tropical or sub-tropical grassland	9	0.5
Temperate or sub-polar grassland	10	0.1
Sub-polar or polar shrubland-lichen-moss	11	0.03
Sub-polar or polar grassland-lichen-moss	12	0.03
Sub-polar or polar barren-lichen-moss	13	0.03
Wetland	14	0.25
Cropland	15	0.25
Barren lands	16	0.03
Urban	17	2
Water	18	1e-3
Snow and ice	19	1.3 10e-3

Text S1: Monin-Obukhov Similarity theory

Under near-neutral atmospheric conditions over horizontally homogeneous and flat terrain, the logarithmic wind profile provides a reasonable approximation of the vertical variation of wind speed and is given by

$$\bar{u}_z = \frac{u_*}{k}\ln\left(\frac{z}{z_0}\right), \tag{S1}$$

where $\bar{u}_z$ denotes the time-averaged wind speed at height z, and u_* is the friction velocity.

Based on dimensional analysis, MOST extends the logarithmic wind profile to account for the thermal stratification in the atmospheric surface layer [1]. Within the atmospheric surface layer, the dimensionless wind shear and temperature gradient are written as

$$\phi_m\left(\frac{z}{L}\right) = \frac{kz}{u_*}\frac{\partial\bar{u}}{\partial z}, \tag{S2}$$

$$\phi_h\left(\frac{z}{L}\right) = \frac{kz}{\theta_*}\frac{\partial\bar{\theta}}{\partial z}, \tag{S3}$$

where ϕ_m, and ϕ_h are the dimensionless wind shear and temperature gradient, respectively, θ_* is the temperature scale. The Obukhov length scale, L, is defined as follows:

$$L = -\frac{u_*^3\bar{\theta}_m}{kg\overline{(w'\theta')}_s}, \tag{S4}$$

where $\bar{\theta}_m$ is the mean potential temperature, g is the acceleration due to gravity, and $\overline{(w'\theta')}_s$ is the surface sensible heat flux. Negative value of L corresponds to unstable conditions characterized by a positive upward heat flux with buoyancy-driven turbulence, whereas positive values indicate stable stratification due to radiative cooling with buoyancy-suppressed turbulence. In the limit $L \to \infty$, the ABL approaches neutral stability.

Integrating Equation (S2) between height z_1 and z_2 yields

$$\bar{u}_2 - \bar{u}_1 = \frac{u_*}{k}\left[\ln\left(\frac{z_2}{z_1}\right) - \psi_m\left(\frac{z_2}{L}\right) + \psi_m\left(\frac{z_1}{L}\right)\right], \tag{S5}$$

where ψ_m is the integrated stability correction function for momentum defined as follows:

$$\psi_m\left(\frac{z}{L}\right) = \int_0^{\frac{z}{L}} \frac{1-\phi_m(\xi)}{\xi} d\xi, \tag{S6}$$

with $\xi = \frac{z}{L}$.

Setting $z_1 = z_0$ leads to

$$\bar{u}_z = \frac{u_*}{k}\left[\ln\left(\frac{z}{z_0}\right) - \psi_m\left(\frac{z}{L}\right) + \psi_m\left(\frac{z_0}{L}\right)\right]. \tag{S7}$$

Although estimating z_0 is challenging [2], Equation (S7) remains useful when only a single wind speed measurement is available. If measurements are available at two heights, Equation (S5) can be directly applied without the need to estimate z_0.

Similarly, integrating the heat similarity between z_1 and z_2 gives

$$\bar{\theta}_2 - \bar{\theta}_1 = \frac{\theta_*}{k}\left[\ln\left(\frac{z_2}{z_1}\right) - \psi_h\left(\frac{z_2}{L}\right) + \psi_h\left(\frac{z_1}{L}\right)\right], \tag{S8}$$

where the temperature similarity function ψ_h is defined as

$$\psi_h\left(\frac{z}{L}\right) = \int_0^{\frac{z}{L}} \frac{1-\phi_h(\xi)}{\xi} d\xi. \tag{S9}$$

Several forms of $\phi_{m,h}$ have been proposed in the literature based on different experimental datasets [3]. For unstable conditions ($L < 0$), we adopt the commonly used formulation of Dyer and Hicks [4], expressed as follows:

$$\phi_m = (1-16\xi)^{-\frac{1}{4}}, \qquad \phi_h = (1-16\xi)^{-\frac{1}{2}}, \tag{S10}$$

with the corresponding integrated forms given by

$$\psi_m = 2\ln\left(\frac{1+x}{2}\right) + \ln\left(\frac{1+x^2}{2}\right) - 2\tan^{-1}(x) + \frac{\pi}{2}, \qquad \psi_h = 2\ln\left(\frac{1+x^2}{2}\right), \tag{S11}$$

where $x = (1-16\xi)^{\frac{1}{4}}$.

Under stable conditions ($L > 0$), the parameterization of Beljaars and Holtslag [5] is used:

$$\phi_m = 1 + a\xi + b\xi(1+c-d\xi)\exp(-d\xi), \tag{S12}$$

with constants $a = 1,\ b = 2/3\,,\ c = 5$, and $d = 0.35$. The corresponding integrated similarity functions are given by

$$\psi_m = -b\left(\xi - \frac{c}{d}\right)\exp(-d\xi) - a\xi - \frac{bc}{d}, \tag{S13}$$

$$\psi_h = -b\left(\xi - \frac{c}{d}\right)\exp(-d\xi) - \left(1 + \frac{2}{3}a\xi\right)^{\frac{3}{2}} - \frac{bc}{d} + 1. \tag{S14}$$

Estimating the flux quantities required to determine the Monin–Obukhov length remains challenging [6]. As an alternative, atmospheric stability may be characterized using the gradient Richardson number [2] defined as follows:

$$\mathrm{Ri} = \frac{g}{\bar{\theta}_m}\frac{\frac{\partial\bar{\theta}}{\partial z}}{\left(\frac{\partial\bar{u}}{\partial z}\right)^2} \tag{S15}$$

Between two temperature measurement heights, z_{t_1} and z_{t_2}, the vertical temperature gradient can be approximated at the geometric mean height $z_{t_m} = \sqrt{z_{t_1} z_{t_2}}$ by assuming a logarithmic profile and applying a finite-difference approximation [7]:

$$\frac{\partial\bar{\theta}}{\partial z} = \frac{\Delta\bar{\theta}}{z_{t_m}\ln\left(z_{t_2}/z_{t_1}\right)}, \tag{S16}$$

where $\Delta\bar{\theta} = \bar{\theta}_2 - \bar{\theta}_1$.

Applying a similar approximation for the wind speed gradient yields the bulk Richardson number,

$$\mathrm{Ri_b} = \frac{g}{\bar{\theta}_m}\frac{\Delta\bar{\theta}}{(\Delta\bar{u})^2}\frac{\left[z_{u_m}\ln\left(z_{u_2}/z_{u_1}\right)\right]^2}{z_{t_m}\ln\left(z_{t_2}/z_{t_1}\right)}, \tag{S17}$$

where $\Delta\bar{u} = \bar{u}_2 - \bar{u}_1$, and z_{u_m} is the geometric mean wind measurement height. The potential temperature difference is approximated as

$$\Delta\bar{\theta} = \Delta\bar{T} + \Gamma_d\Delta z, \tag{S18}$$

with $\Gamma_d = 0.0098\ \mathrm{Km}^{-1}$ denoting the dry adiabatic lapse rate [8].

Finally, by combining Equations (S4), (S5), (S8), and (S17), the Monin–Obukhov length can be expressed as a function of the bulk Richardson number, given by

$$\mathrm{Ri_b} = \frac{z_{Ri}}{L} \frac{\left[\ln\left(\frac{z_{t_2}}{z_{t_1}}\right) - \psi_h\left(\frac{z_{t_2}}{L}\right) + \psi_h\left(\frac{z_{t_1}}{L}\right)\right]}{\left[\ln\left(\frac{z_{u_2}}{z_{u_1}}\right) - \psi_m\left(\frac{z_{u_2}}{L}\right) + \psi_m\left(\frac{z_{u_1}}{L}\right)\right]^2}, \tag{S19}$$

where $\mathrm{Ri_b}$ denotes bulk Richardson number and $z_{Ri} = \frac{\left[z_{u_m} \ln(z_{u_2}/z_{u_1})\right]^2}{z_{t_m} \ln(z_{t_2}/z_{t_1})}$. Equation (S19) is transcendental in L and must be solved iteratively.

References

1. Foken T, Mauder M. Micrometeorology: Springer; 2008.
2. Brotzge JA, Crawford KC. Estimating Sensible Heat Flux from the Oklahoma Mesonet. Journal of Applied Meteorology. 2000;39(1):102-16.
3. Högström U. Non-dimensional wind and temperature profiles in the atmospheric surface layer: A re-evaluation. Boundary-Layer Meteorology. 1988;42(1):55-78.
4. Dyer AJ, Hicks BB. Flux-gradient relationships in the constant flux layer. Quarterly Journal of the Royal Meteorological Society. 1970;96(410):715-21.
5. Beljaars ACM, Holtslag AAM. Flux Parameterization over Land Surfaces for Atmospheric Models. Journal of Applied Meteorology and Climatology. 1991;30(3):327-41.
6. Lee TR, Buban M, Meyers TP. Application of Bulk Richardson Parameterizations of Surface Fluxes to Heterogeneous Land Surfaces. Monthly Weather Review. 2021;149(10):3243-64.
7. Arya PS. Introduction to Micrometeorology: Academic Press; 2001.
8. Stull R. Practical Meteorology: An Algebra-based Survey of Atmospheric Science. British Columbia.: Univ. of British Columbia.; 2018. 940 p.

Text S2: Theoretical wind shear exponent

For engineering applications, the power-law is commonly used to extrapolate wind speed from a reference height $z_1$to target hub height z_2:

$$\bar{u}_2 = \bar{u}_1 \left(\frac{z_2}{z_1}\right)^{\alpha}, \tag{S20}$$

where α is the shear exponent, which depends on atmospheric stability and surface roughness.

In practice, α is assumed constant, with a typical value of $\alpha = 1/7$, corresponding to neutral atmospheric stability conditions over a flat terrain. Alternatively, a stability and surface roughness dependent shear exponent α can be derived from MOST [1, 2] as follows:

$$\alpha = \left(\frac{u_*}{\bar{u}_z k}\right) \phi_m \left(\frac{z}{L}\right). \tag{S21}$$

Because $\bar{u}_z$ at the extrapolation height is unknown, it can be estimated using the integrated wind profile between z_1 and z as follows:

$$\alpha = \left\{\frac{u_*}{k u_1 + u_* \left[\ln\left(\frac{z}{z_1}\right) - \psi_m\left(\frac{z}{L}\right) + \psi_m\left(\frac{z_1}{L}\right)\right]}\right\} \phi_m \left(\frac{z}{L}\right). \tag{S22}$$

If the reference height is set equal to the roughness length ($z_1 = z_0$), the shear exponent simplifies to

$$\alpha = \frac{\phi_m \left(\frac{z}{L}\right)}{\ln\left(\frac{z}{z_0}\right) - \psi_m\left(\frac{z}{L}\right) + \psi_m\left(\frac{z_0}{L}\right)}. \tag{S23}$$

This MOST formulation of the shear exponent indicates that the WSE is height dependent. For practical applications, a representative shear exponent between two heights z_2 and z_3 can be estimated at an height z_m [1]:

$$\alpha = \left\{\frac{u_*}{k u_1 + u_* \left[\ln\left(\frac{z_m}{z_1}\right) - \psi_m\left(\frac{z_m}{L}\right) + \psi_m\left(\frac{z_1}{L}\right)\right]}\right\} \phi_m \left(\frac{z_m}{L}\right), \tag{S24}$$

where $z_m = \frac{1}{2}\left[\left(\frac{z_2+z_3}{2}\right) + \sqrt{z_2 z_3}\right]$.

References

1. Irwin JS. A theoretical variation of the wind profile power-law exponent as a function of surface roughness and stability. Atmospheric Environment (1967). 1979;13(1):191-4.
2. Panofsky HA, Blackadar AK, McVehil GE. The diabatic wind profile. Quarterly Journal of the Royal Meteorological Society. 1960;86(369):390-8.

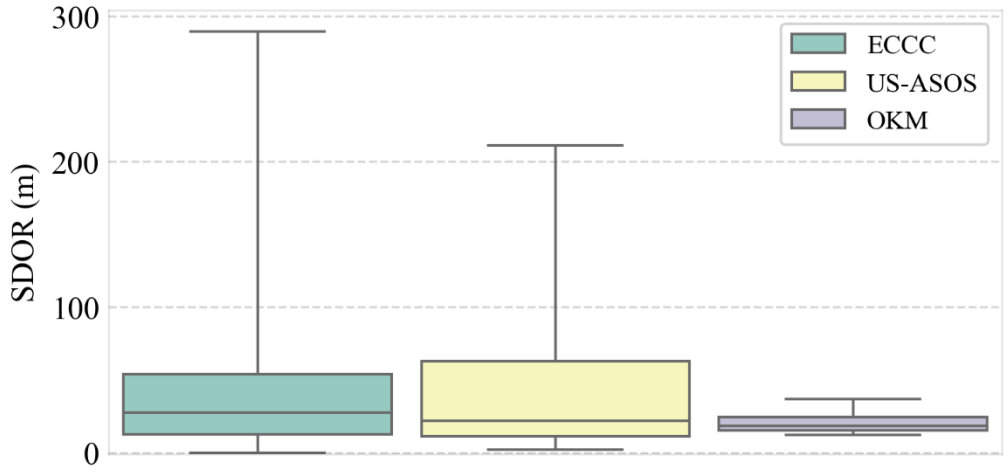

Figure S1. Boxplot of standard deviation of orography height (SDOR) for ECCC, US-ASOS, and OKM. The SDOR is one of the ERA5 geophysical datasets used to parametrize sub-grid-scale processes and is used in this study as a measure of terrain complexity within the station grid cell.

.

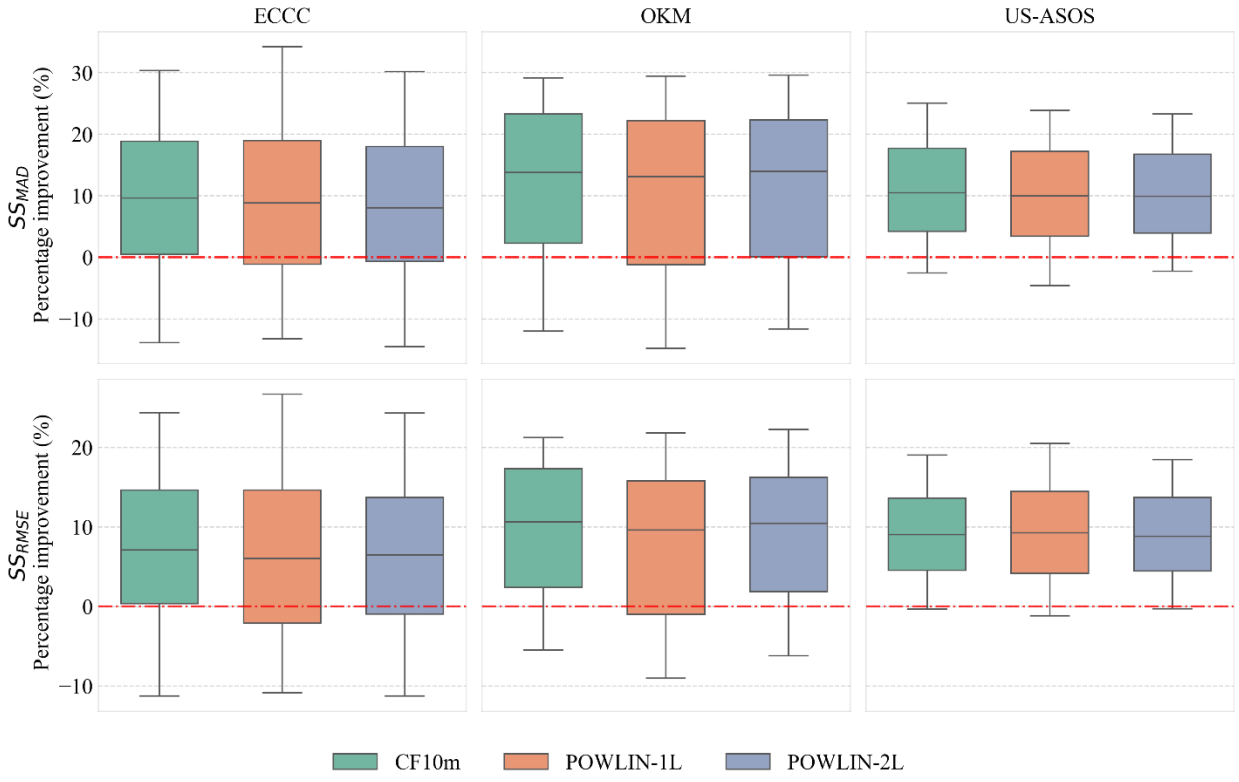

Figure S2. Boxplot of skill scores for CF10m, POWLIN-1L, and POWLIN-2L. Overall, the different model configurations led to positive skill scores at most stations, indicating an improvement relative to ERA5. The improvements in MAD and RMSE are generally more pronounced with lower variability at the US-ASOS stations. The magnitude and variability of the improvement remain relatively consistent across the different model configurations.

Table S3. Skill scores stratified by ecoregion [1] for the ECCC, US-ASOS, and OKM station networks.

Ecoregion	Metrics	CF10m	POWLIN-1L	POWLIN-2L	N
Arctic Cordillera	$N(SS_{MAD} > 0)$ (%)	**100.000**	**100.000**	**100.000**	1
	$N(SS_{RMSE} > 0)$ (%)	**100.000**	**100.000**	**100.000**	1
	SS_{MAD} (%)	**18.958**	13.839	17.354	1
	SS_{RMSE} (%)	**20.633**	11.876	18.692	1
Coastal	$N(SS_{MAD} > 0)$ (%)	56.627	57.831	**65.060**	83
	$N(SS_{RMSE} > 0)$ (%)	**62.651**	61.446	**62.651**	83
	SS_{MAD} (%)	**4.997**	3.988	3.381	83
	SS_{RMSE} (%)	3.075	4.561	**5.098**	83
Eastern Temperate Forests	$N(SS_{MAD} > 0)$ (%)	87.026	86.627	**87.425**	501
	$N(SS_{RMSE} > 0)$ (%)	**90.818**	90.619	**90.818**	501
	SS_{MAD} (%)	**14.202**	13.552	12.778	501
	SS_{RMSE} (%)	11.234	**11.511**	10.862	501
Great Plains	$N(SS_{MAD} > 0)$ (%)	**81.356**	76.998	77.240	413
	$N(SS_{RMSE} > 0)$ (%)	**85.230**	77.966	81.114	413
	SS_{MAD} (%)	**8.336**	7.104	7.380	413
	SS_{RMSE} (%)	**7.189**	6.469	6.867	413
Hudson Plains	$N(SS_{MAD} > 0)$ (%)	55.556	**66.667**	**66.667**	9
	$N(SS_{RMSE} > 0)$ (%)	66.667	66.667	**77.778**	9
	SS_{MAD} (%)	**11.683**	9.003	7.353	9
	SS_{RMSE} (%)	3.880	**8.665**	6.886	9
Marine West Coast Forests	$N(SS_{MAD} > 0)$ (%)	**87.037**	83.333	83.333	54
	$N(SS_{RMSE} > 0)$ (%)	**81.481**	75.926	75.926	54
	SS_{MAD} (%)	**11.908**	11.217	11.151	54
	SS_{RMSE} (%)	6.597	**6.937**	5.932	54
Mediterranean California	$N(SS_{MAD} > 0)$ (%)	**94.737**	89.474	92.982	57
	$N(SS_{RMSE} > 0)$ (%)	91.228	87.719	**92.982**	57
	SS_{MAD} (%)	13.663	**14.259**	14.153	57
	SS_{RMSE} (%)	10.521	**11.588**	11.243	57
North American Deserts	$N(SS_{MAD} > 0)$ (%)	**81.481**	**81.481**	79.630	108
	$N(SS_{RMSE} > 0)$ (%)	82.407	**86.111**	83.333	108
	SS_{MAD} (%)	6.492	6.320	**6.732**	108
	SS_{RMSE} (%)	6.309	**6.860**	6.378	108
Northern Forests	$N(SS_{MAD} > 0)$ (%)	**76.953**	71.484	71.875	256
	$N(SS_{RMSE} > 0)$ (%)	**75.000**	68.359	71.484	256
	SS_{MAD} (%)	**10.712**	8.984	9.321	256
	SS_{RMSE} (%)	**7.697**	5.483	6.302	256
Northwestern Forested Mountains	$N(SS_{MAD} > 0)$ (%)	**71.831**	64.789	**71.831**	71
	$N(SS_{RMSE} > 0)$ (%)	63.380	**66.197**	**66.197**	71
	SS_{MAD} (%)	**7.662**	7.417	6.968	71
	SS_{RMSE} (%)	3.940	**4.551**	3.989	71

Southern Semi-Arid Highlands	$N(SS_{MAD} > 0)$ (%)	**50.000**	**50.000**	**50.000**	2
	$N(SS_{RMSE} > 0)$ (%)	**100.000**	**100.000**	**100.000**	2
	SS_{MAD} (%)	2.583	**4.206**	2.354	2
	SS_{RMSE} (%)	3.540	**4.978**	4.355	2
Taiga	$N(SS_{MAD} > 0)$ (%)	80.000	**86.667**	**86.667**	15
	$N(SS_{RMSE} > 0)$ (%)	**86.667**	**86.667**	**86.667**	15
	SS_{MAD} (%)	9.132	**9.629**	7.867	15
	SS_{RMSE} (%)	**7.731**	6.434	6.618	15
Temperate Sierras	$N(SS_{MAD} > 0)$ (%)	**100.000**	**100.000**	**100.000**	2
	$N(SS_{RMSE} > 0)$ (%)	**100.000**	**100.000**	**100.000**	2
	SS_{MAD} (%)	10.890	5.581	**13.544**	2
	SS_{RMSE} (%)	7.616	6.528	**8.994**	2
Tropical Humid Forests	$N(SS_{MAD} > 0)$ (%)	**100.000**	72.727	**100.000**	11
	$N(SS_{RMSE} > 0)$ (%)	**100.000**	81.818	**100.000**	11
	SS_{MAD} (%)	**17.445**	11.173	17.323	11
	SS_{RMSE} (%)	13.192	8.224	**15.145**	11
Tundra	$N(SS_{MAD} > 0)$ (%)	0.000	0.000	0.000	3
	$N(SS_{RMSE} > 0)$ (%)	0.000	0.000	0.000	3
	SS_{MAD} (%)	-12.660	-9.395	-11.552	3
	SS_{RMSE} (%)	-7.834	-7.931	-5.602	3

Notes: The best values for each network, metric, and ecoregion are in boldface. SS_{MAD} and SS_{RMSE} denote the skill scores computed using ERA5 as the reference baseline. $N(SS_{MAD} > 0)$ and $N(SS_{RMSE} > 0)$ represent the proportion of stations for which the skill score is positive.

References

1. North American Environmental Atlas - Terrestrial Ecoregions: Level I [Internet]. Commission for Environmental Cooperation (CEC) 2021 [cited 2026/05/13]. Available from: https://www.cec.org/north-american-environmental-atlas/terrestrial-ecoregions-level-i/.

Table S4. Median values of the performance metrics computed across the different models, height intervals, and atmospheric stability regimes at the TALLDB stations.

Height interval	Metrics	Stability regime	CF10m	ERA5	POWLIN-1L	POWLIN-2L
10-40 m a.g.l	CRMSE	Neutral	2.901	3.148	2.921	**2.866**
		Stable	1.749	1.816	**1.724**	1.727
		Unstable	1.79	1.845	1.785	**1.772**
	MAD	Neutral	1.904	2.115	**1.768**	1.784
		Stable	1.017	1.643	**0.995**	1.114
		Unstable	1.13	1.357	**1.082**	1.09
	PCC	Neutral	**0.554**	0.455	0.541	0.552
		Stable	0.377	0.309	**0.387**	0.378
		Unstable	**0.506**	0.404	0.505	0.51
	RMSE	Neutral	3.278	3.933	**3.263**	3.313
		Stable	1.873	2.334	**1.843**	1.86
		Unstable	1.925	2.362	1.901	**1.867**
40-100 m a.g.l	CRMSE	Neutral	3.613	3.462	**3.436**	3.554
		Stable	2.59	2.313	**2.182**	2.428
		Unstable	2.216	2.218	**2.125**	2.153
	MAD	Neutral	2.288	2.311	**2.083**	2.242
		Stable	1.43	1.694	**1.294**	1.4
		Unstable	1.333	1.4	**1.201**	1.275
	PCC	Neutral	0.511	0.485	0.508	**0.525**
		Stable	0.307	0.318	**0.376**	0.319
		Unstable	0.483	0.385	0.484	**0.49**
	RMSE	Neutral	3.794	3.877	**3.578**	3.791
		Stable	2.653	2.857	**2.271**	2.52
		Unstable	2.31	2.62	**2.145**	2.179

Note: The ERA5 Monin–Obukhov length was used to classify atmospheric stability into three regimes [1]: unstable ($-0.5 < L^{-1} < -0.002$), neutral ($-0.002 \leq L^{-1} \leq 0.002$) and, stable conditions ($0.002 < L^{-1} < 0.5$). The values of the best-performing model for each height interval and metric are in boldface.

References

1. Debnath M, Moriarty P, Krishnamurthy R, Bodini N, Newsom R, Quon E, et al. Characterization of wind speed and directional shear at the AWAKEN field campaign site. Journal of Renewable and Sustainable Energy. 2023;15(3):033308.

Table S5. Performance metrics computed at each Tall Tower Dataset station

Station name	Height	CRMSE				MAD				PCC				RMSE			
		CF10m	ERA5	POWLIN-1L	POWLIN-2L	CF10m	ERA5	POWLIN-1L	POWLIN-2L	CF10m	ERA5	POWLIN-1L	POWLIN-2L	CF10m	ERA5	POWLIN1L	POWLIN-2L
BROOKHAVEN	10	1.816	**1.74**	1.757	1.78	1.129	1.179	**1.067**	1.101	0.28	0.186	**0.283**	0.28	2.011	1.933	**1.931**	1.981
	50	2.614	2.561	**2.396**	2.455	1.736	1.645	**1.586**	1.598	**0.174**	0.134	0.167	0.16	2.619	2.563	**2.416**	2.455
	85	3.199	3.086	**2.927**	3.11	2.361	**2.115**	2.211	2.205	0.129	**0.15**	0.136	0.129	3.405	**3.196**	3.215	3.244
BUTLER GRADE	31	2.986	3.081	**2.947**	3.132	2.15	3.095	**2.012**	2.095	0.801	**0.826**	0.81	0.782	3.755	4.704	**3.525**	3.727
	45	**2.971**	3.087	2.984	3.115	2.027	2.913	**1.956**	2.011	0.819	**0.841**	0.823	0.806	3.593	4.598	**3.461**	3.585
	62	**2.942**	3.065	3.007	2.946	1.98	2.828	1.945	**1.893**	0.831	**0.852**	0.83	0.836	3.46	4.512	**3.426**	3.313
CHINOOK	50	1.969	1.899	**1.85**	1.882	1.3	**1.188**	1.232	1.311	0.832	0.827	**0.843**	0.84	2.284	**1.927**	2.112	2.221
KENNEWICK	24	3.694	3.851	**3.651**	3.814	2.796	3.891	**2.492**	2.638	0.745	**0.768**	0.753	0.722	5.033	6.1	**4.721**	5.009
	37	**3.203**	3.266	3.215	3.371	2.208	3.209	**2.046**	2.153	0.738	**0.763**	0.737	0.706	3.927	4.963	**3.787**	4.055
MEGLER	53	1.965	2.042	**1.878**	1.892	1.155	1.34	**1.1**	1.152	0.752	**0.777**	0.752	0.755	1.968	2.144	**1.912**	1.892
NWTC M2	10	**2.218**	2.418	2.223	2.22	0.955	1.234	**0.941**	1.011	**0.555**	0.413	0.549	0.551	2.271	2.812	2.361	**2.24**
	20	**2.406**	2.587	2.429	2.431	1.081	1.356	**1.05**	1.107	**0.567**	0.463	0.559	0.558	**2.458**	3.034	2.6	2.462
	50	2.76	2.858	2.745	**2.728**	1.326	1.588	**1.241**	1.251	0.559	0.512	0.573	**0.574**	2.817	3.41	2.997	**2.798**
	80	2.975	2.959	**2.872**	2.916	1.482	1.645	**1.324**	1.428	0.537	0.526	**0.572**	0.551	3.003	3.488	3.115	**2.962**
NWTC M4	10	**2.087**	2.288	2.092	2.093	1.039	1.398	**1.035**	1.142	**0.554**	0.41	0.553	0.551	2.088	2.832	2.106	**2.103**
	100	3.195	3.005	**2.924**	3.149	1.829	1.713	**1.493**	1.754	0.518	0.52	**0.556**	0.526	3.249	3.54	**2.945**	3.175
	15	**2.362**	2.542	2.375	2.375	1.207	1.531	**1.167**	1.262	**0.55**	0.439	0.544	0.543	**2.365**	3.146	2.402	2.377
	26	**2.46**	2.626	2.466	2.479	1.33	1.561	**1.222**	1.348	**0.568**	0.477	0.564	0.558	**2.461**	3.219	2.492	2.482
	30	2.456	2.575	**2.438**	2.445	1.386	1.592	**1.264**	1.387	**0.541**	0.457	**0.541**	0.536	2.459	3.155	2.459	**2.451**
	50	2.884	2.955	2.828	**2.818**	1.6	1.777	**1.414**	1.524	0.543	0.495	0.554	**0.558**	2.884	3.626	2.887	**2.818**
	76	3.072	3.013	**2.915**	2.971	1.74	1.764	**1.475**	1.651	0.527	0.51	**0.554**	0.545	3.087	3.633	**2.958**	2.973
	80	3.059	3.024	**2.912**	2.969	1.734	1.677	**1.475**	1.653	0.547	0.527	**0.574**	0.563	3.083	3.585	**2.941**	2.977
	88	3.046	2.949	**2.849**	2.969	1.748	1.659	**1.469**	1.67	0.544	0.533	**0.576**	0.557	3.088	3.491	**2.871**	2.987
NWTC M5	10	**2.184**	2.237	2.227	2.203	**1.046**	1.328	1.088	1.047	**0.413**	0.337	0.399	0.403	**2.229**	2.737	2.266	2.232
	100	3.494	3.22	**3.179**	3.535	1.993	1.809	**1.748**	2.007	0.362	0.352	**0.382**	0.349	3.528	3.514	**3.184**	3.576
	15	**2.4**	2.418	2.423	**2.4**	1.235	1.389	1.24	**1.208**	**0.379**	0.318	0.365	0.368	**2.418**	2.861	2.449	2.419
	30	2.786	2.791	2.757	**2.749**	1.457	1.607	1.399	**1.366**	**0.407**	0.36	0.402	0.399	2.807	3.307	2.818	**2.8**
	38	2.814	2.782	2.746	**2.734**	1.509	1.613	1.421	**1.389**	**0.407**	0.363	**0.407**	0.405	2.818	3.244	2.786	**2.765**

	41	3.056	2.99	2.973	**2.956**	1.679	1.733	1.579	**1.546**	**0.35**	0.307	0.346	0.346	3.068	3.494	3.035	**3.007**
	55	3.106	3.026	**2.982**	3.012	1.686	1.711	**1.544**	1.581	0.397	0.365	**0.405**	0.399	3.107	3.472	**3.022**	3.023
	61	3.211	3.084	**3.051**	3.114	1.795	1.731	**1.624**	1.703	0.374	0.347	**0.383**	0.374	3.212	3.467	**3.074**	3.115
	74	3.277	3.124	**3.075**	3.211	1.81	1.745	**1.612**	1.758	0.368	0.35	**0.387**	0.365	3.279	3.506	**3.102**	3.212
	80	3.366	3.204	**3.156**	3.32	1.855	1.77	**1.656**	1.822	0.389	0.37	**0.405**	0.384	3.371	3.581	**3.18**	3.323
	87	3.38	3.176	**3.137**	3.362	1.875	1.769	**1.662**	1.861	0.388	0.375	**0.405**	0.378	3.392	3.532	**3.155**	3.372
OAK RIDGE	10	0.988	1.151	1.016	**0.967**	0.556	0.93	0.595	**0.552**	**0.678**	0.514	0.661	0.669	1.093	1.451	1.18	**1.085**
	100	1.593	1.728	**1.303**	1.485	0.973	1.224	**0.786**	0.876	0.68	0.641	**0.709**	0.689	1.594	2.071	**1.308**	1.503
	30	1.244	1.446	1.136	**1.092**	0.674	1.176	0.639	**0.61**	**0.659**	0.508	0.649	0.653	1.341	1.867	1.245	**1.17**
OSU	34	1.761	1.793	1.619	**1.571**	1.605	1.97	**1.494**	1.585	0.635	0.629	**0.638**	0.632	2.383	2.698	**2.21**	2.239
	46	1.934	1.962	1.749	**1.743**	1.474	1.771	**1.328**	1.425	0.603	0.603	**0.608**	0.603	2.288	2.585	**2.066**	2.145
PARK FALLS	30	1.238	1.255	1.148	**1.092**	1.23	1.529	**1.053**	1.135	**0.79**	0.745	0.789	0.784	1.726	1.941	**1.542**	1.573
SEVEN MILE	15	2.527	3.292	2.526	**2.445**	2.593	4.356	**2.156**	2.471	0.843	0.751	0.844	**0.853**	3.789	5.783	**3.444**	3.645
	30	2.534	3.38	2.613	**2.542**	2.35	4.409	**2.243**	2.554	0.847	0.758	0.849	**0.855**	3.543	5.852	**3.54**	3.754
TROUTDALE	30	2.039	2.024	**2.004**	2.024	0.934	0.952	0.867	**0.864**	0.525	0.521	**0.53**	0.502	2.039	2.051	**2.011**	2.041
WASCO	30	2.178	**2.052**	2.145	2.239	**1.685**	2.226	1.715	1.761	0.701	**0.733**	0.701	0.678	**2.734**	3.174	2.796	2.864

Note: The values of the best-performing model for each station and metrics are in boldface.

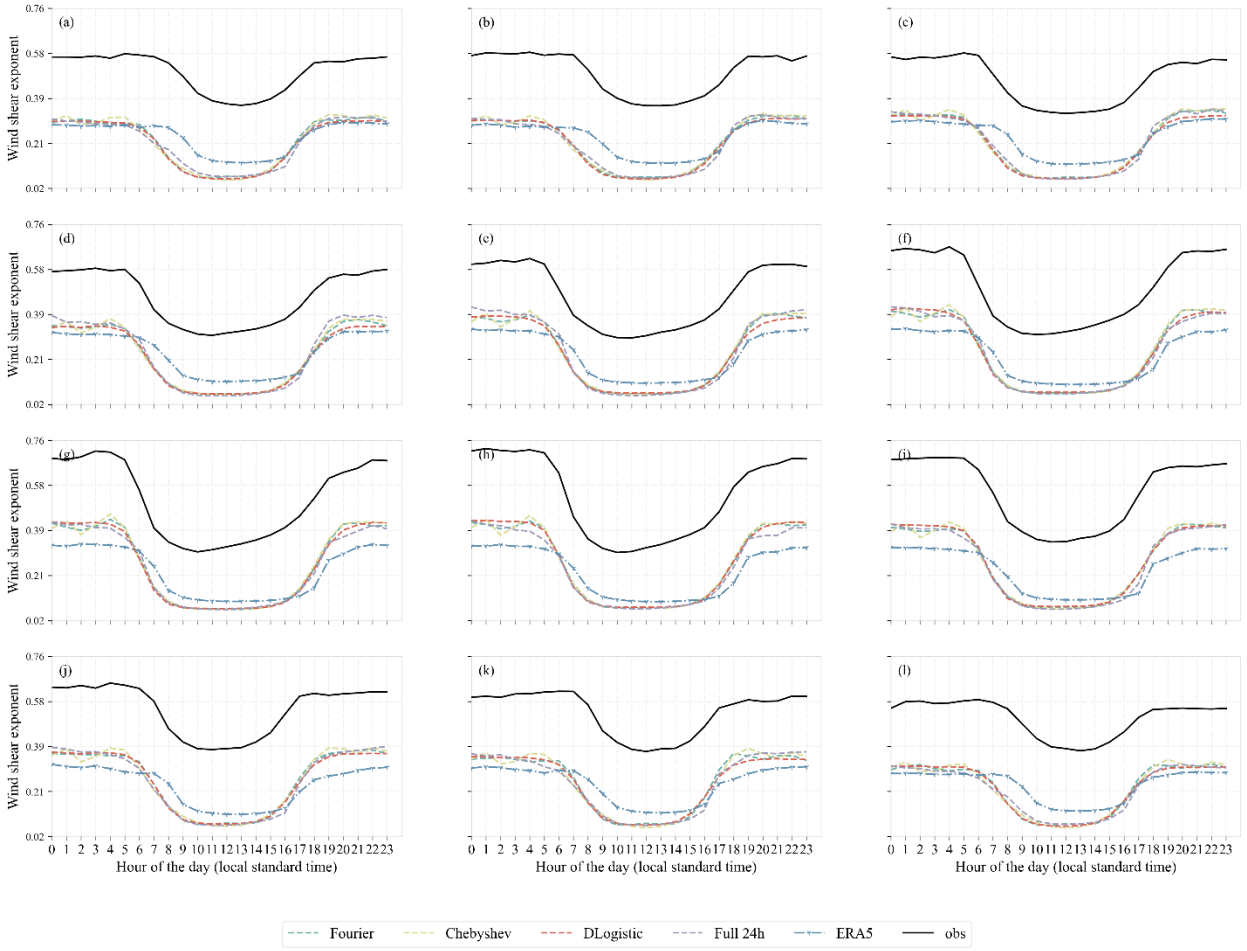

Figure S3. Monthly diurnal cycle of wind shear between 10 m and 85 m AGL at BROOKHAVEN site. Observations are compared with ERA5 and POWLIN-1L predictions (color-coded). The POWLIN-1L diurnal variability is represented using three formulations: Fourier series, Chebyshev series, and full 24h prediction. Panel (a) shows January, and the subsequent panels present the remaining months of the year.

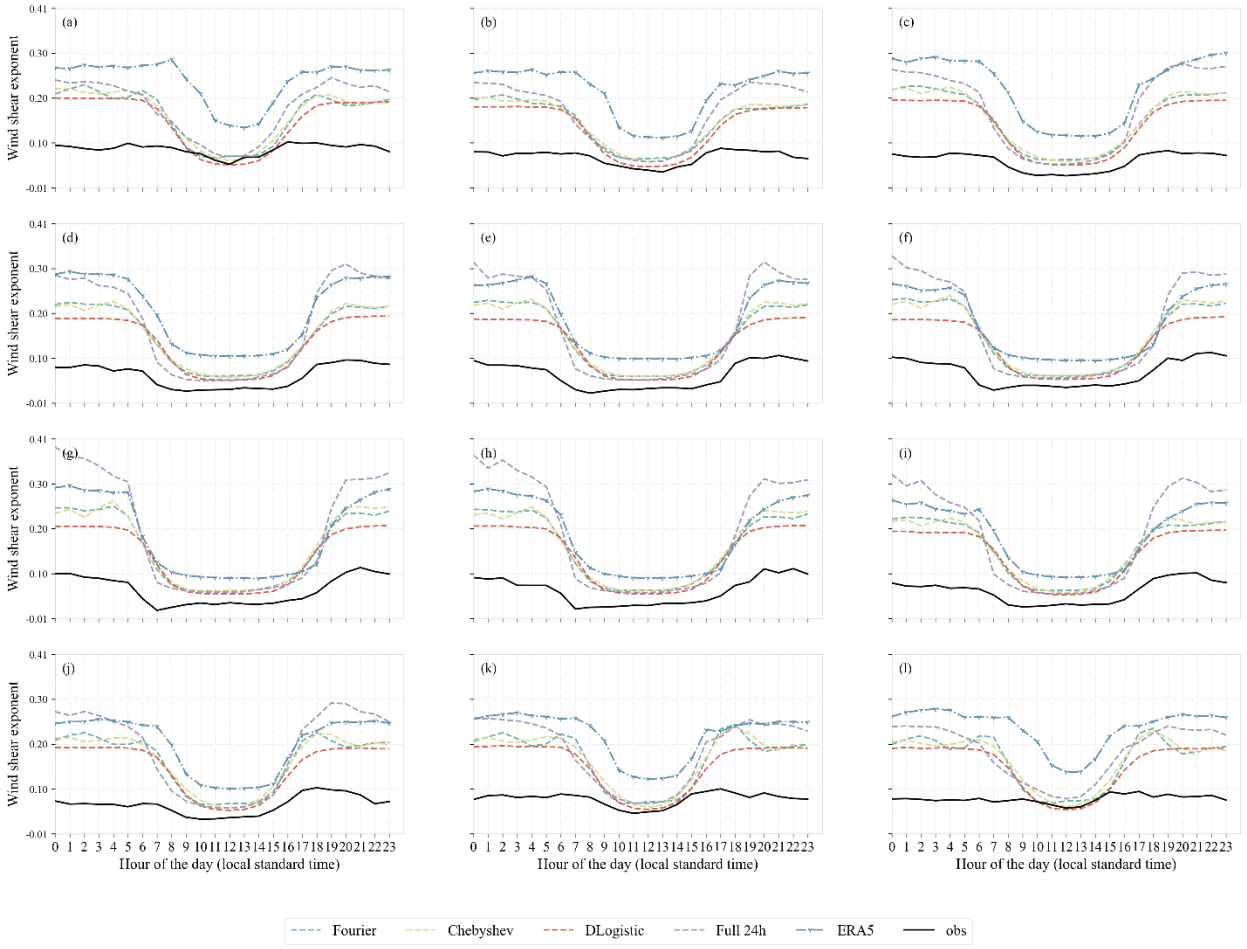

Figure S4. Monthly diurnal cycle of wind shear between 31 m and 62 m AGL at BUTLER GRADE site. Observations are compared with ERA5 and POWLIN-1L predictions (color-coded). The POWLIN-1L diurnal variability is represented using three formulations: Fourier series, Chebyshev series, and full 24h prediction. Panel (a) shows January, and the subsequent panels present the remaining months of the year.

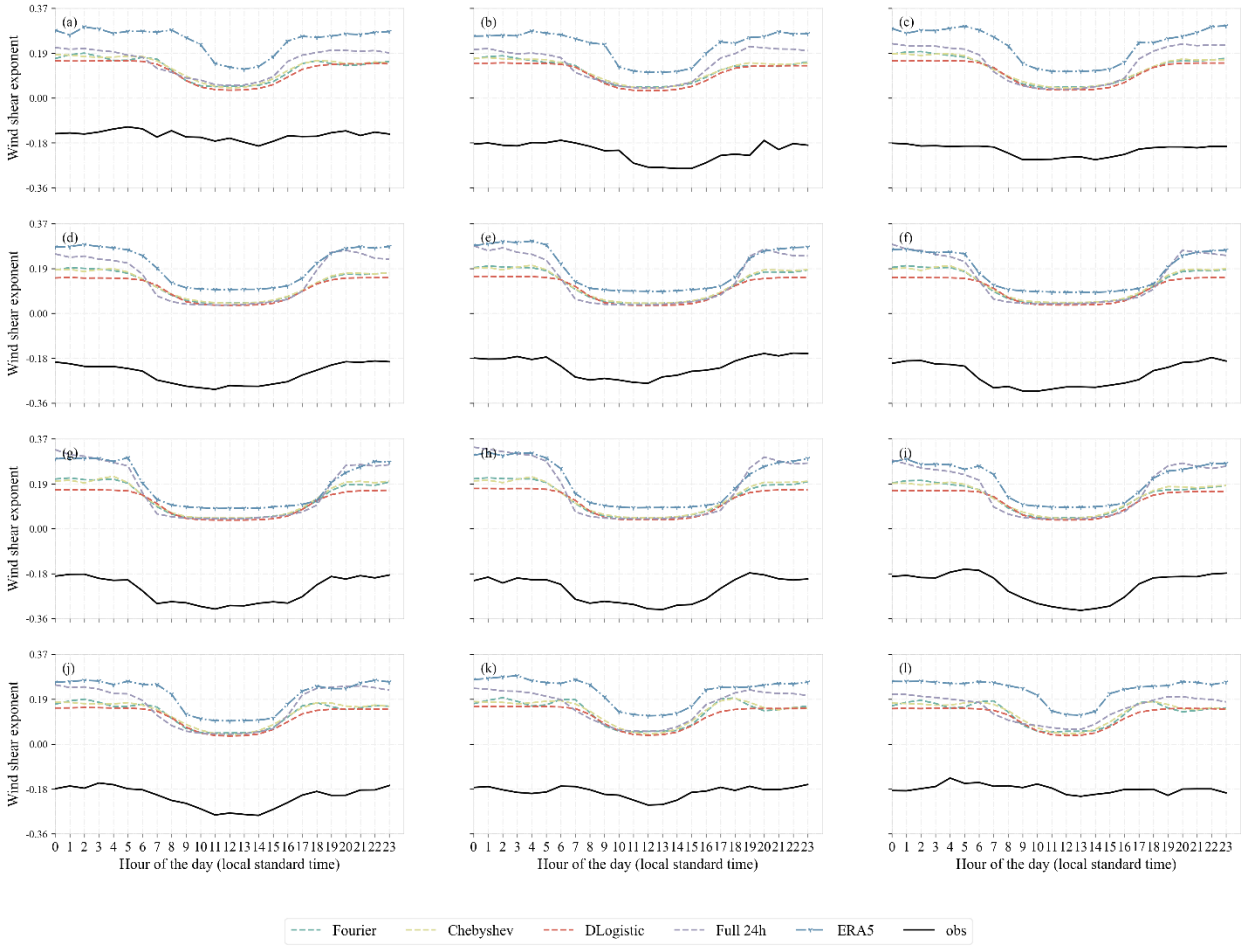

Figure S5. Monthly diurnal cycle of wind shear between 24 m and 37 m AGL at KENNEWICK site. Observations are compared with ERA5 and POWLIN-1L predictions (color-coded). The POWLIN-1L diurnal variability is represented using three formulations: Fourier series, Chebyshev series, and full 24h prediction. Panel (a) shows January, and the subsequent panels present the remaining months of the year.

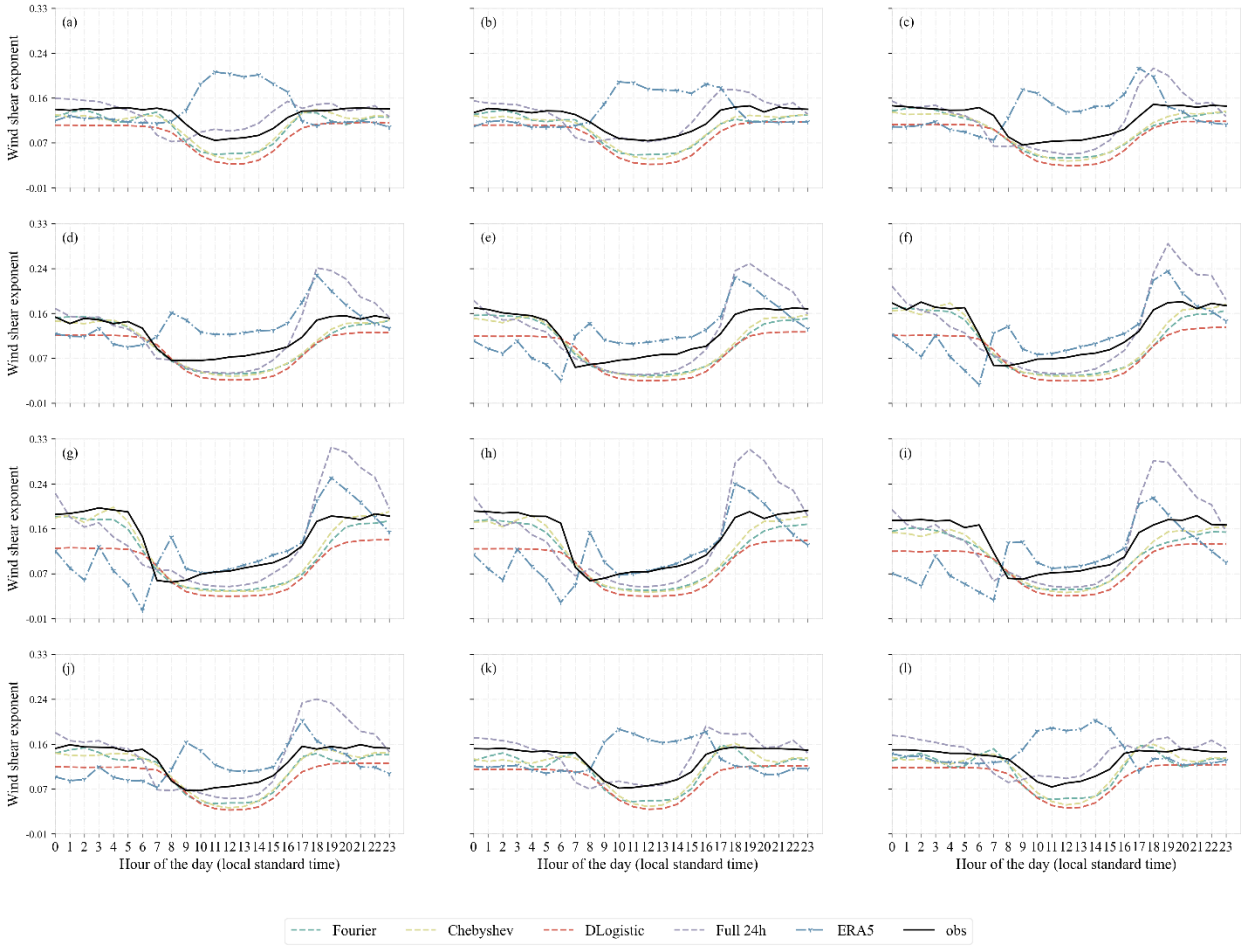

Figure S6. Monthly diurnal cycle of wind shear between 10 m and 80 m AGL at NWTC M2 site. Observations are compared with ERA5 and POWLIN-1L predictions (color-coded). The POWLIN-1L diurnal variability is represented using three formulations: Fourier series, Chebyshev series, and full 24h prediction. Panel (a) shows January, and the subsequent panels present the remaining months of the year.

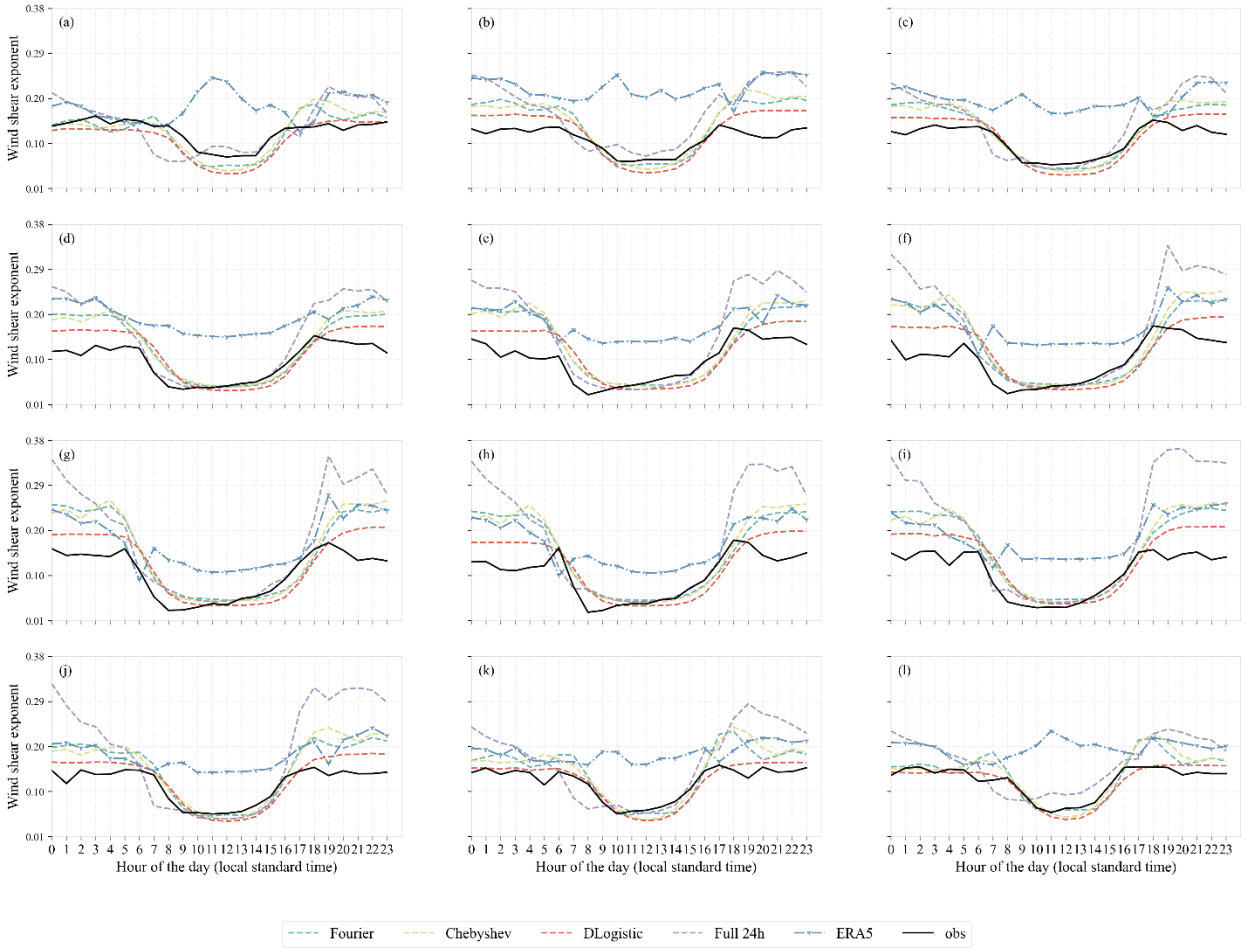

Figure S7. Monthly diurnal cycle of wind shear between 10 m and 100 m AGL at NWTC M5 site. Observations are compared with ERA5 and POWLIN-1L predictions (color-coded). The POWLIN-1L diurnal variability is represented using three formulations: Fourier series, Chebyshev series, and full 24h prediction. Panel (a) shows January, and the subsequent panels present the remaining months of the year.

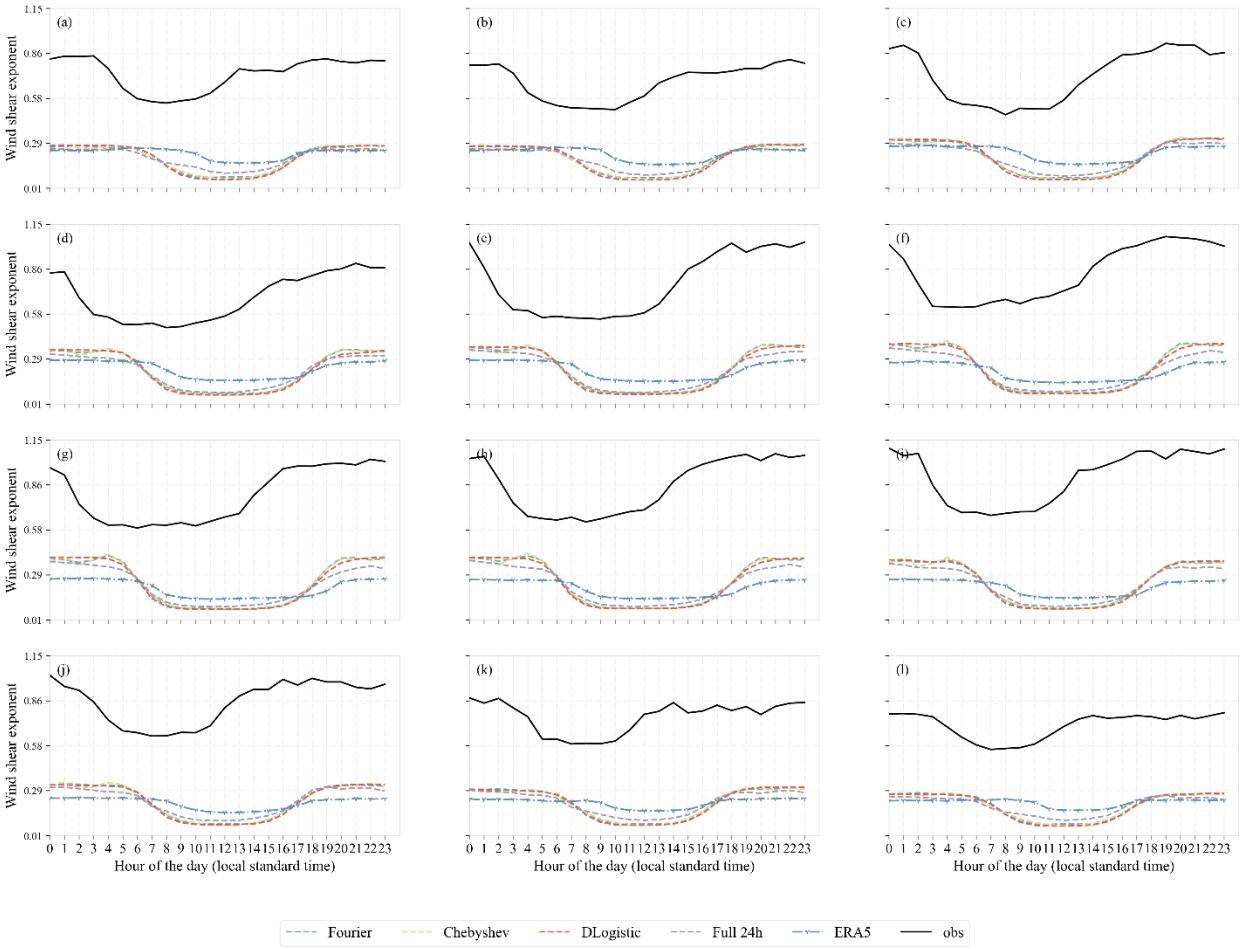

Figure S8. Monthly diurnal cycle of wind shear between 34 m and 46 m AGL at OSU site. Observations are compared with ERA5 and POWLIN-1L predictions (color-coded). The POWLIN-1L diurnal variability is represented using three formulations: Fourier series, Chebyshev series, and full 24h prediction. Panel (a) shows January, and the subsequent panels present the remaining months of the year.

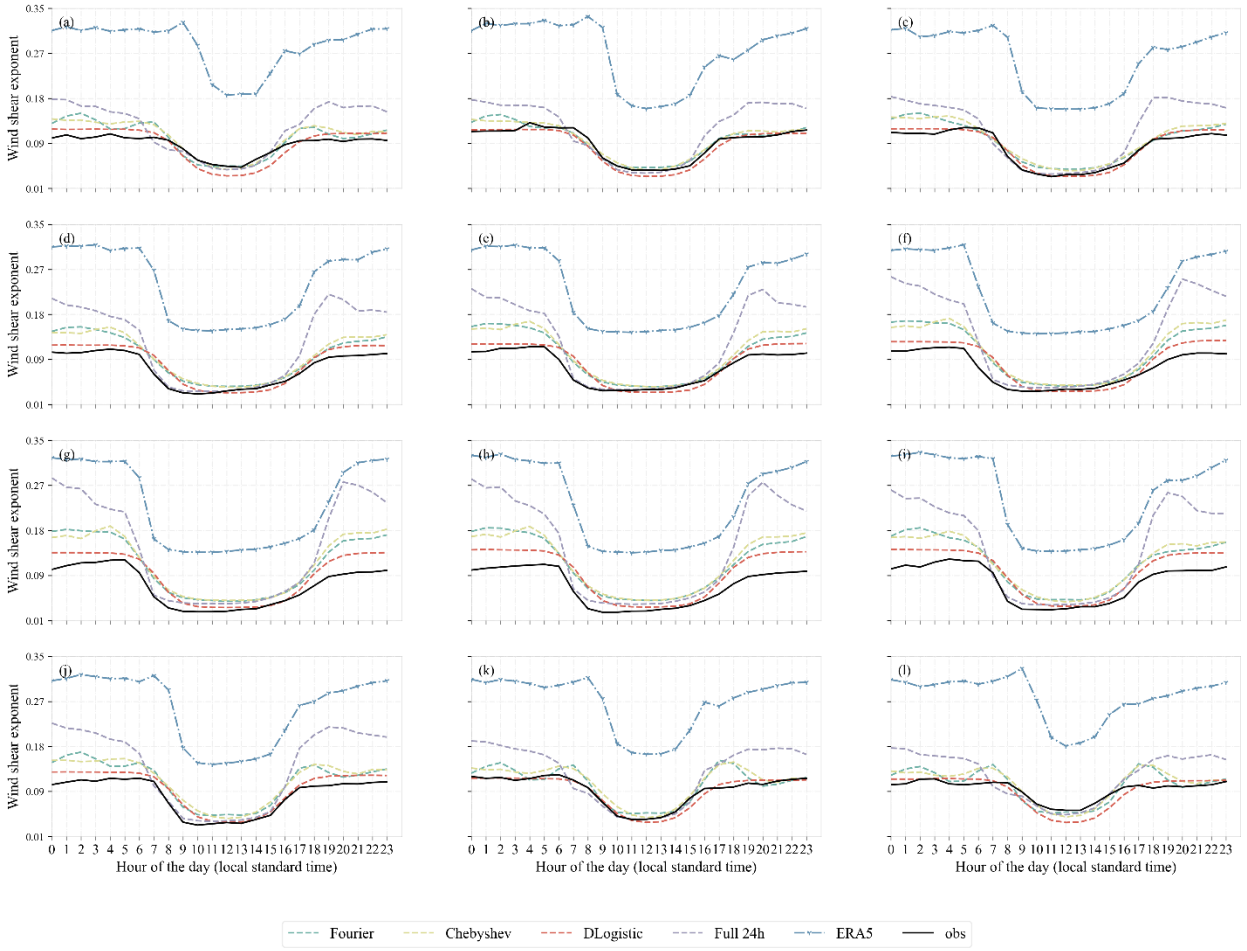

Figure S9. Monthly diurnal cycle of wind shear between 15 m and 30 m AGL at SEVEN MILE site. Observations are compared with ERA5 and POWLIN-1L predictions (color-coded). The POWLIN-1L diurnal variability is represented using three formulations: Fourier series, Chebyshev series, and full 24h prediction. Panel (a) shows January, and the subsequent panels present the remaining months of the year.